Materials Science in Semiconductor Processing 70 (2017) 207–212

Contents lists available at ScienceDirect

Materials Science in Semiconductor Processing

journal homepage: www.elsevier.com/locate/mssp

Si:iscsi-vii/istdm2016

Displacement current of Au/p-diamond Schottky contacts

Toshichika Aoki[a,*], Tokuyuki Teraji[b], Yasuo Koide[b], Kenji Shiojima[a]

[a] Graduate School of Engineering, University of Fukui, 3-9-1 Bunkyo, Fukui 910-8507, Japan
[b] National Institute for Materials Science, 1-1 Namiki, Tsukuba, Ibaraki 305-0044, Japan

ARTICLE INFO

Keywords:
p-diamond
p-GaN
Schottky contact
I–V characteristic
AC operation

ABSTRACT

In this study, the displacement current of Au/p-diamond Schottky contacts was studied by comparing them with low-Mg-doped p-GaN Schottky contacts. In the current–voltage (*I–V*) characteristics, the current was proportional to the voltage sweep speed at $V > -1.5$ V. The differential output waveform was obtained through AC operation. Therefore, the displacement current was dominant in the low voltage region where in the true current was extremely small due to the large Schottky barrier height of 1.57 eV. The memory effect, due to the charge and discharge of localized acceptor-type deep-level defects, was negligible in the *I–V* curve. A clear AC differential signal was confirmed. This suggested that the interface defect density of the p-diamond contacts was very small compared to the p-GaN contacts. Hence, p-diamond Schottky contacts were expected to be a good candidate for a key device such as a phase modulator in a wireless transmitter.

1. Introduction

Wide bandgap materials such as GaN and SiC are readily used in commercially available products such as GaN/InGaN blue light-emitting diodes, laser diodes [1], radio-frequency AlGaN/GaN high electron mobility transistors [2–4], SiC power Schottky diodes, and MOSFETs [5,6]. These materials are of interest for developing the next-generation of high-power switching applications for GaN devices and mass production of SiC devices. In addition to these materials, the superior durability of diamond over SiC and GaN has attracted considerable attention for higher-power device applications in harsh environments such as outer space. A breakdown voltage as high as 4.9 kV has been achieved for 4H–SiC Schottky barrier diodes [7]. GaN and diamond have been utilized to fabricate 1-kV-class Schottky diodes [8,9]. However, compared to Si, crystal growth of wide bandgap materials is difficult because of the high defect densities in their crystal structures. SiC bulk crystals are produced using a sublimation method, and the active layers are homoepitaxially grown on the SiC substrate. In the SiC crystal, the main defects are threading dislocations caused by mixing polytypes and stacking faults. The typical dislocation density (D_{dis}) in 4H–SiC is approximately 10^3 cm^{-2}[10]. GaN is grown on a different material substrate. A large lattice mismatch induces a large D_{dis}. Typical D_{dis} in a GaN crystal is approximately 10^9 cm^{-2} on SiC substrates [11]. Recently, GaN has been grown homoepitaxially on freestanding GaN substrates. However, D_{dis} is still approximately 10^7 cm^{-2}[12], In the case of homoepitaxial diamond films, D_{dis} is reportedly 10^4–10^5 cm^{-2} when the substrates are conventional Ib (100) diamond crystals and may become smaller using high-quality IIa (100) substrates [13].

These dislocations generally affected the current transport at the material semiconductor interface. For example, in the metal-GaN contact, a large leakage current and a weak metal-work function dependence were observed [14,15]. Moreover, p-GaN contacts are not as well understood as n-GaN contacts. Initially, the contacts tended to exhibit very leaky Schottky characteristics, but exhibited high series resistances due to poor crystal quality [16]. Consequently, the mechanism of current flow through the interface had not been established, and the exact value of the Schottky barrier height ($q\phi_B$) had not yet been estimated. We reported improved leakage characteristics for low-Mg-doped Ni/p-GaN Schottky contacts with a $q\phi_B$ as large as 2.4 ± 0.2 eV obtained from current–voltage (*I–V*) measurements [17]. Such a high $q\phi_B$ led to the flow of a displacement current, as it dominated the true current in the *I–V* characteristics when the diode was switched off. In other words, analysis of displacement current was meaningful to understand current transport at the metal-semiconductor interface with a considerable amount of defects.

The $q\phi_B$ of a p-diamond Schottky barrier diode, fabricated using a vacuum ultraviolet-ozone treatment is as large as the Ni/p–GaN contact [9], which suggests a substantial contribution from a displacement current in the current transport. In this study, we extend this analysis of displacement current to the p-type diamond Schottky contact. The purpose of this study is to prove the degree of displacement current appearing from the p-diamond Schottky diode through the quantitative analysis and compare it with our previous results of

* Corresponding author.
E-mail address: aoki0529@u-fukui.ac.jp (T. Aoki).

http://dx.doi.org/10.1016/j.mssp.2016.12.012
Received 26 July 2016; Received in revised form 2 December 2016; Accepted 13 December 2016
Available online 06 January 2017

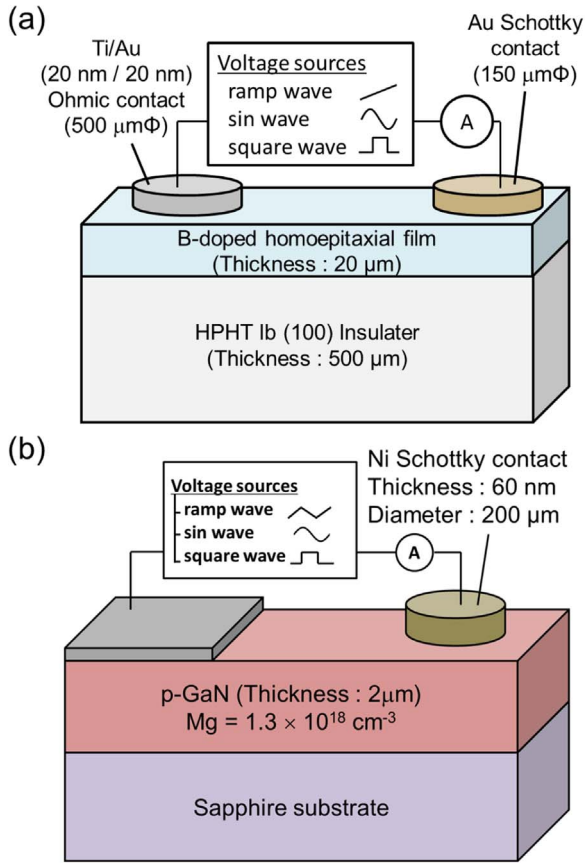

Fig. 1. Device structures with measurement circuits of the (a) Au/p-diamond and (b) low-Mg-doped Ni/p–GaN contacts.

the p-GaN contacts [18]. We conduct *I–V* measurements by varying the voltage sweep speed (*I–*v_{sweep}) and changing the sweep direction. We also conduct AC operation with square and sinusoidal wave inputs. We report that a clear AC signal is achieved without the memory effect.

2. Experimental procedure

2.1. Sample preparation

20-μm-thick boron-doped p-diamond films were homoepitaxially grown on high-pressure, high-temperature type Ib diamond (100) substrates by microwave plasma chemical vapor deposition, as shown in Fig. 1(a). The sample was prepared by following the technique described in a previous report [9]. First, the diamond surface was terminated by hydrogenation through exposure to hydrogen plasma. Then, Ti/Au (20/20 nm thick, 500 μmϕ) ohmic contacts were on the four corners of the homoepitaxial diamond surface by using electron beam (EB) evaporation. Vacuum ultraviolet light was irradiated under an oxygen atmosphere to convert the hydrogen-terminated bare surface selectively into oxygen termination. Finally, Au Schottky contacts (50-nm-thick, 150 μmϕ) were deposited at the middle part of the oxygen-terminated surface by EB evaporation. For comparison with the diamond sample, we recalled the *I–V* characteristics of the Ni/p–GaN contacts in Ref. 18. The diodes were fabricated in the same manner as our previous report [17]. 2-μm-thick, low-Mg-doped GaN (Mg: 1×10^{18} cm^{-3}) films were grown on sapphire substrates by metalorganic chemical vapor deposition, as shown in Fig. 1(b). After cleaning with acetone and ethanol solvents, followed by a hydrochloric acid surface treatment, Ni Schottky contacts (60-nm-thick, 200 μmϕ) were deposited by EB evaporation. Finally, large-area InGa ohmic electrodes were formed on the p-GaN surfaces without annealing.

2.2. Electrical measurements

Herein, we describe the measurement sequence that was conducted in this study. After illumination of the samples with white light, *I–*v_{sweep} measurements were performed in total darkness using a voltage sweep ranging from 0 to −5 V (first sweep of decreasing voltage) at the absolute v_{sweep} values of 0.01, 0.1, and 1 V/s. Then, the second *I–V* measurements were made immediately after the first sweep with the voltage sweep direction reversed starting from −5 to +5 V (sweep of increasing voltage). Subsequently, AC operation was demonstrated by applying an input square wave voltage at a frequency of 0.01 Hz to clearly observe a differential signal and a sinusoidal wave voltage at 0.1 Hz for p-diamond and 0.02 Hz for p-GaN to observe a differential signal in a single frequency domain. We used a pico-ampere (pA) meter with a maximum sampling frequency of 10 Hz.

The displacement current was defined by the following equation:

$$I = C\frac{dV}{dt}, \quad (1)$$

where *C* is the depletion layer capacitance. As expected from Eq. (1), when we applied an AC signal, a differential output signal was observed [18]. Therefore, it might be suitable as a new modulator that can provide a diode operation with differential function.

However, a large density of acceptor-type deep-level defects (D_{deep}) was found in the vicinity of the interface [19]. We conducted two forward voltage sweeps in quick succession. D_{deep} led to a change in the *I–V* curves between the first and second voltage sweeps. We called this phenomenon the memory effect, because it was caused by the charge and discharge of D_{deep}[20]. The memory effect was a serious problem under AC operation [18].

In an ideal diode, the *I–V* characteristics obey the thermionic emission model [21], and the displacement current can be added. In order to observe the displacement current for a wide voltage range, a high $q\phi_B$, reverse and leakage currents smaller than the displacement current, and a large *C* value are required. However, in the fablicated diode, as indicated in the previous report [18], the *I–V* characteristics are not ideal. The reverse and leakage currents, the memory effect caused by the interfacial defects, the linearity as a functional of voltage sweep speed in Eq. (1), and the frequency response are all causes for concern. A detail characterization of the displacement current is necessary for analysis of the real AC operation.

3. Results and discussion

3.1. I–V characteristics

Fig. 2 shows the *I–*v_{sweep} characteristics for the (a) p-diamond and (b) p-GaN samples. The solid lines with markers are the measured currents from the *I–V* sweeps. In the p-diamond sample, the first voltage sweep we conducted from 0 to −5 V demonstrated a good linear relationship until the current exponentially increased at approximately −2 V. When we extrapolated the linear potions, the obtained $q\phi_B$ and n values ranged from 1.49 to 1.57 eV and 2.31–2.50, respectively, depending on v_{sweep} and the sweep direction. When the voltage range was 0–−2 V with a v_{sweep} at 0.01 V/s, the current was below the noise floor level. With v_{sweep} at 0.1 and 1 V/s, the current was proportional to v_{sweep}. In this voltage region, because the true current was extremely small, we detected the displacement current as expected from Eq. (1). For the second sweep, the same *I–V* curve was obtained and mimicked the first one up to −2.5 V because the memory effect was negligible. This suggested that the surface defect density was very small compared to p-GaN. Although the voltage was directed forward at approximately −1.5 V, the direction of the current was reversed. We found that the reverse current flow was approximately constant in the voltage range between −1.5 V and +5 V. In addition, the absolute value of the current was proportional to the sweep speed and was the same as that of the

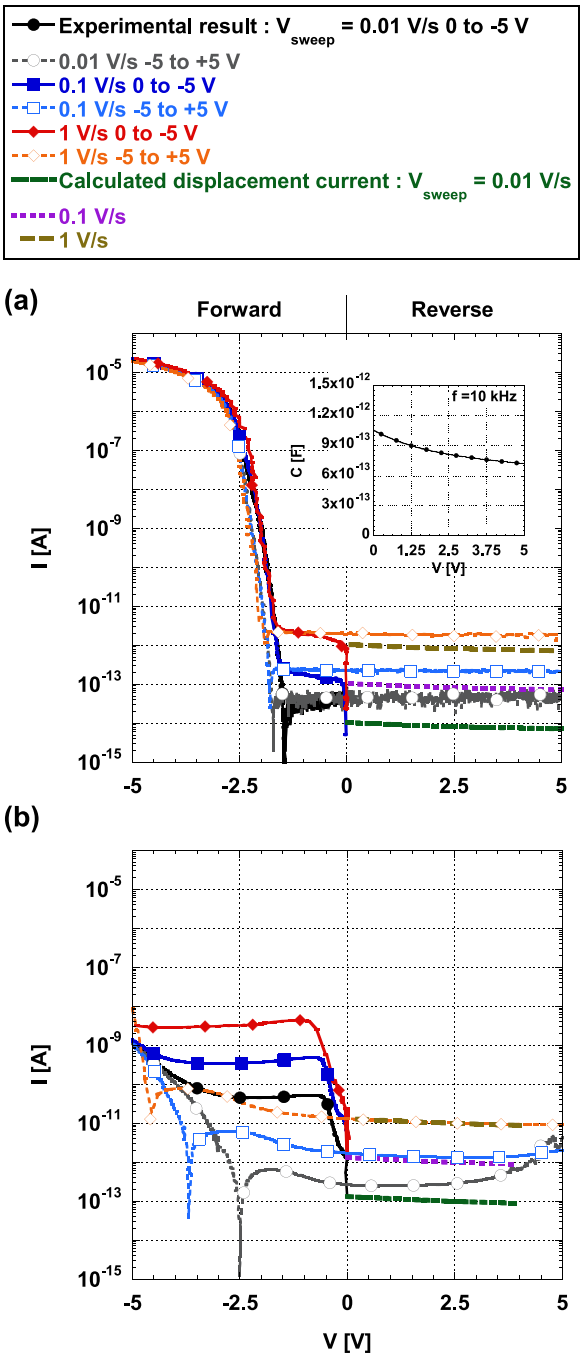

Fig. 2. Typical I–v_{sweep} characteristics for the (a) p-diamond and (b) p-GaN samples (after Ref.18) in a semi-log plot. The lines with marks are experimental results with voltage sweeps (from 0 to −5 for the first, −5 to +5 V for the second). The dashed lines without marks are displacement currents that are calculated using the measured C in the inset.

first sweep. Therefore, these currents could also be considered as displacement currents. The dashed lines without marks in Fig. 2(a) indicate displacement currents, which were calculated based on Eq. (1) using the measured C values in the capacitance–voltage (C–V) characteristics as shown in the inset. The C–V measurement was conducted at 10 kHz with an impedance analyzer in this study, and the C value at 0 V was a constant value between 3 kHz and 400 kHz. When the v_{sweep} was 0.1 and 1 V/s, the calculated displacement current values were about two times smaller than the measured current values. In the p-type diamond contact, due to a large activation energy of boron acceptors, the measured C value became larger at a much lower frequency than the impedance analyzer could handle. On the other hand, a very low-frequency C–V measurement such as a C measurement with a ramp-function voltage could be detected using the I–v_{sweep} measurement, which can induce a large capacitance. Therefore, the difference between the C values in low and high frequencies contributed to the difference between the calculated and measured currents. There was a large difference between the C values when the v_{sweep} was 0.01 V/s because the actual current was below the noise level of the measurement. The observation of the displacement current was quantitatively confirmed.

Next, we compared the I–V results between the diamond and GaN contacts. We referred to the I–V curves of the low-Mg-doped p-GaN Schottky contacts reported in Ref. 18, as shown in Fig. 2(b). The displacement currents were mainly observed in the voltage region from −2.5 to +2.5 V. The calculated displacement currents from the measured capacitance are shown by dashed lines. A good agreement was obtained between the experimental and calculated values. On the other hand, a large difference between the first and second sweeps due to the memory effect was observed. The memory effect could be explained by the capture and emission of holes into accepter-type D_{deep} in the vicinity of the interface, which significantly varied the depletion layer width (W_{dep}) [20]. Furthermore, D_{deep} did not originate from dislocations but from gallium vacancies that were located in the vicinity of the p-GaN surface [19]. In the case of the diamond contacts, since no memory effect was obviously seen, we deduced that a small density of interfacial defects existed and it was less likely due to dislocations. We found that the diamond contact was more suitable than the p-GaN contact to provide diode characteristics with displacement current.

We have explained the current transport mechanism with an energy band diagram for the p-diamond contact, as shown in Fig. 3. We examine the case when the applied voltage is swept from a large forward bias to zero with a constant v_{sweep}. When the forward bias is large, a true current with holes based on thermionic emission is dominant. As the voltage increases, the true current exponentially decreases. At the same time, W_{dep} becomes thicker, and capacitance becomes smaller. In this situation, a displacement current can flow in the opposite direction, but the variation against a bias voltage is much smaller than the true current. Therefore, there is a bias turning point wherein the dominant current switches from true to displacement current. This point is around −1.6 V in the actual I–V curves, as shown in Fig. 2(a). When a further voltage sweep is conducted in the reverse direction through V =0 V, the polarity of the true current is inverted; however, the displacement current continually flows.

3.2. AC operation

Figs. 4 and 5 show the experimental results of the AC operation with square-wave inputs for the p-diamond and p-GaN samples to observe a clear differential signal. Fig. 4(a) shows an input voltage waveform and Fig. 4(b) and (c) show the output current signals when

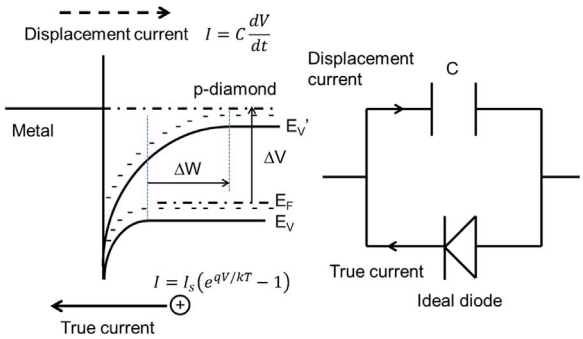

Fig. 3. Schematic of the current transport mechanism with an energy band diagram and an equivalent circuit diagram of the metal/p-diamond interface.

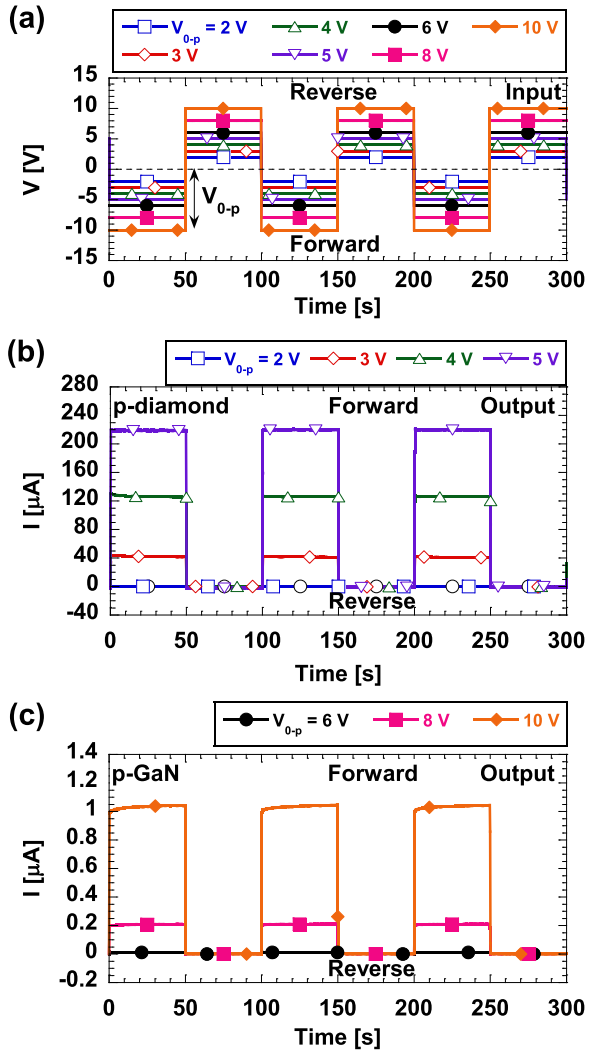

Fig. 4. AC operation with large square-wave inputs: (a) input voltage waveform, output currents waveforms (b) for p-diamond (open square is for V_{0-p} =2 V, open diamond is for V_{0-p} =3 V, open triangle is for V_{0-p} =4 V, and open inverted triangle is for V_{0-p} =5 V) and (c) p-GaN (filled circle is for V_{0-p} =6, filled square is for V_{0-p} =8 V, and filled diamond is for V_{0-p} =10 V) samples. These symbols are labeled at every 10th to 20th data points in the figure.

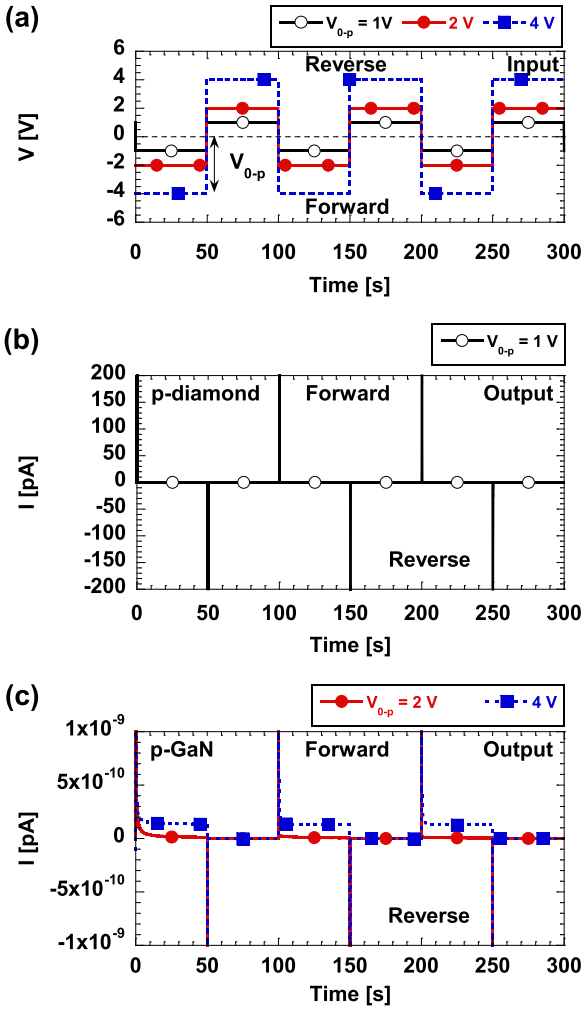

Fig. 5. AC operation with small square-wave inputs: (a) input voltage waveform, output current waveform (b) for p-diamond (open circle is for V_{0-p} =1 V) and (c) p-GaN (filled circle is for V_{0-p} =2 V and filled square is for V_{0-p} =4 V) samples. These symbols are labeled at every 10th to 20th data points in the figure.

the amplitude of the input signal (V_{0-p}) is 2–5 V for p-diamond and 6–10 V for p-GaN, respectively. When V_{0-p} is larger than 2 V for the p-diamond and larger than 6 V for the p-GaN, the output currents are rectified by a conventional diode function for both samples. This is possible because most of the time, the operation is in the true-current dominant region. Next, we observe AC operation in the lower voltage region. Fig. 5(a) shows input voltage waveforms; (b) and (c) show the output current signals when V_{0-p} is 1 V for p-diamond and 2–4 V for p-GaN, respectively. In this case, we observe spikes at the point of the input voltage polarity change for both samples. This can be interpreted by the differential operation originating from the displacement current. For more quantitative analysis, the rise and fall times of the input square wave are measured to be 0.4 ms by using an oscilloscope. The slope (dV/dt) is estimated to be 5×10^3 V/s when V_{0-p} is 1 V. When a large forward bias is applied, the C–V analyzer can not accurately measure the value of C, due to a large forward current. We estimate the C values from the voltage slope of 5×10^3 V/s and the peak current of 2×10^{-10} A. A value of 4×10^{-14} F is obtained, which is much smaller than we expect from the C–V results. This discrepancy may be responsible for the under estimation of the current peak due to a low sampling frequency of the pA meter. Therefore, we conduct AC measurements in a single frequency domain (with a sine wave) as a second measurement.

When the input signal is large, Fig. 6(a) shows an input voltage waveform, whereas Fig. 6(b) and (c) show the output current signals when the amplitude of V_{0-p} is 1–2 V for p-diamond and 6–10 V for p-GaN, respectively. As expected, conventional rectified in-phase sine waves are observed in the output current of both samples because the true current is dominant.

Next, we observe the AC operation with a smaller input signal. Fig. 7(a) shows input voltage waveforms, whereas (b) and (c) show output current signals when V_{0-p} is 0.5 V for p-diamond and p-GaN, respectively. In the output signals, a non-rectified cosine wave is clearly seen for the p-diamond sample. The differential signal due to the displacement current is confirmed without the memory effect. In contrast, in the p-GaN sample, we can see a non-rectified cosine component and a rectified sine-component. The peak height of the sine wave decreases with time. This occurs when the first wave reaches the diode junction and large tunneling current flows to the depletion layer. Simultaneously, a small portion of the current can be injected into D_{deep} and W_{dep} becomes wider. When the second forward-bias wave reaches the diode, the peak of the current significantly decreased. Because each wave can precede the hole injection to the defect, the peak height becomes reduces. Therefore, the memory effect is also confirmed by AC operation. These results indicate that the p-diamond contact provides a clear differential signal with less memory effect.

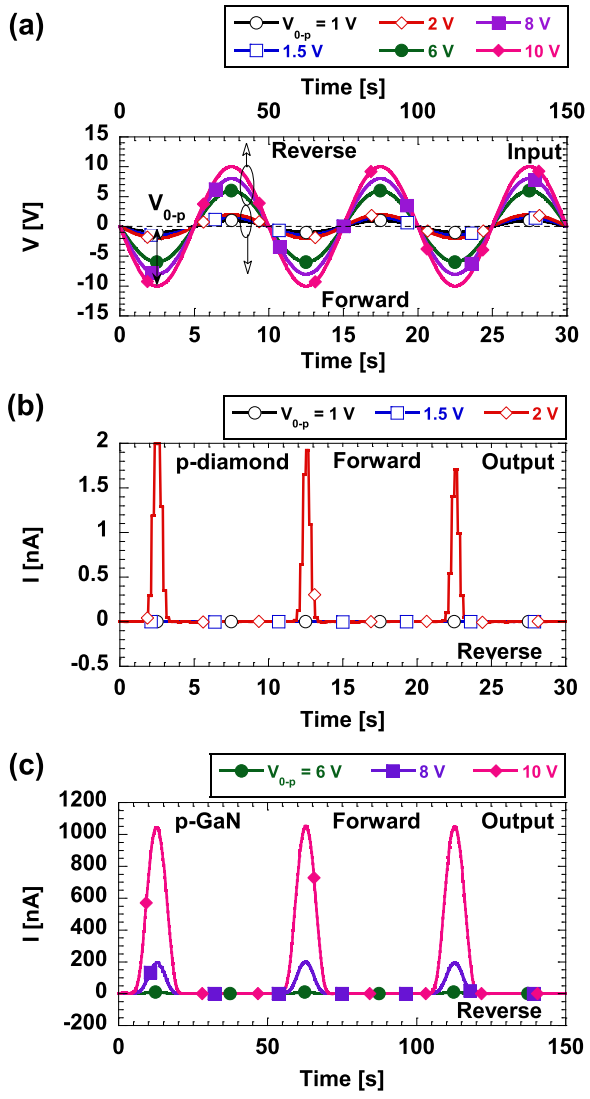

Fig. 6. AC operation when a large sinusoidal wave is applied: (a) input voltage waveform, output current waveform (b) for p-diamond (open circle is for V_{0-p} =1 V, open square is for V_{0-p} =1.5 V, and open diamond is for V_{0-p} =2 V) and (c) p-GaN (filled circle is for V_{0-p} =6 V, filled square is for V_{0-p} =8 V and filled diamond is for V_{0-p} =10 V) samples. These symbols are labeled at every 10th to 20th data points in the figure.

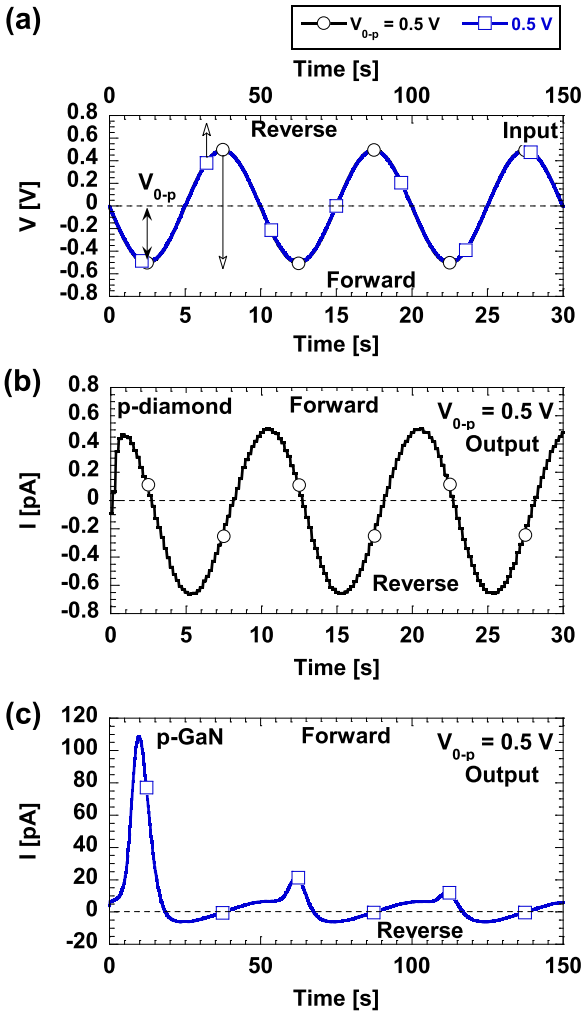

Fig. 7. AC operation when a small sinusoidal wave is applied: (a) input voltage waveform, output current waveforms (b) for p-diamond and (c) p-GaN samples. These symbols are labeled at every 10th to 20th data points in the figure.

Finally, we discuss the actual AC operation of the p-diamond diode. First, these AC results are simply valuable for analysis of the actual AC operation of the diodes. Since we used a pA ammeter in this study, the upper boundary of the measurement frequency is limited by the sampling frequency (10 Hz) of the pA ammeter. However, in the actual diode operation, the upper frequency can be limited by the RC time constant of the diode. In our *C*–frequency measurements, the upper limit is estimated to be 400 kHz in the present device structure. On the other hand, the lower frequency is limited at 2 mHz by the noise level, as shown in Fig. 2.

Second, this diode can function as a key device such as a phase modulator in a wireless transmitter. In a conventional phase modulator, a local signal is modulated by a digital base-band signal using a mixer in a transmitter. Gilbert cell mixers that consist of two-stage differential transistor pairs with a constant current source are widely used. On the other hand, in our proposal, a local signal is applied to the p-diamond diodes, and the measured current becomes an output signal. For example, if we consider the experimental set up that is used in the AC measurements, assuming the amplitude of the local signal is controlled by a digital base-band signal, when the input voltage is larger than 1 V, the in-phase output signal is obtained. When the input voltage is smaller than 0.5 V, the 90°-shift signal is obtained. The p-diamond contact can act as a phase shifter. At this moment, the diamond device cannot accommodate large scale circuits, but this simple structure is sufficient.

4. Conclusions

The displacement currents of p-diamond Schottky contacts were investigated using I–v_{sweep} measurements and AC operation by comparing with p-GaN contacts. We found that the current was proportional to v_{sweep} when the diodes were in the off state.

We also observed a differential output waveform under AC operation when the input voltage amplitude was −0.5 V. Therefore, the displacement current was dominant in the low-voltage region wherein the true current flow was much smaller than that in the p-GaN contacts. In addition, the I–v_{sweep} characteristics showed a negligible memory effect and a clear differential signal for the p-diamond contacts. It was suggested that the interface defect density was much smaller when compared to p-GaN contacts. Hence, p-diamond contacts were expected to be good candidates for a key device such as a phase modulator in a wireless transmitter.

Acknowledgments

Part of this work was supported by a Grant-in-Aid for Scientific

Research (C) 15K05981 and (B) 15H03980 from Ministry of Education, Culture, Sports, Science, and Technology.

References

[1] S. Nakamura, M. Senoh, S. ichi Nagahama, N. Iwasa, T. Yamada, T. Matsushita, H. Kiyoku, Y. Sugimoto, InGaN-based multi-quantum-well-structure laser diodes, Jpn. J. Appl. Phys. 35 (1996) L74–L76. http://dx.doi.org/10.1143/JJAP.35.L74.

[2] U.K. Mishra, P. Parikh, Yi-Feng Wu, AlGaN/GaN HEMTs-an overview of device operation and applications, Proc. IEEE 90 (2002) 1022–1031. http://dx.doi.org/10.1109/JPROC.2002.1021567.

[3] S. Yoshida, H. Ishii, J. Li, D. Wang, M. Ichikawa, A high-power AlGaN/GaN heterojunction field-effect transistor, Solid. State Electron. 47 (2003) 589–592. http://dx.doi.org/10.1016/S0038-1101(02)00419-7.

[4] N.-Q. Zhang, S. Keller, G. Parish, S. Heikman, S.P. DenBaars, U.K. Mishra, High breakdown GaN HEMT with overlapping gate structure, IEEE Electron Device Lett. 21 (2000) 421–423. http://dx.doi.org/10.1109/55.863096.

[5] Q. Wahab, T. Kimoto, A. Ellison, C. Hallin, M. Tuominen, R. Yakimova, A. Henry, J.P. Bergman, E. Janzén, A 3 kV Schottky barrier diode in 4H-SiC, Appl. Phys. Lett. 72 (1998) 445. http://dx.doi.org/10.1063/1.120782.

[6] J.N. Shenoy, J.A. Cooper, M.R. Melloch, High-voltage double-implanted power MOSFET's in 6H-SiC, IEEE Electron Device Lett. 18 (1997) 93–95. http://dx.doi.org/10.1109/55.556091.

[7] R. Singh, J.A. Cooper, M.R. Melloch, T.P. Chow, J.W. Palmour, SiC power Schottky and PiN diodes, IEEE Trans. Electron Devices 49 (2002) 665–672. http://dx.doi.org/10.1109/16.992877.

[8] N. Tanaka, K. Hasegawa, K. Yasunishi, N. Murakami, T. Oka, 50A vertical GaN Schottky barrier diode on a free-standing GaN substrate with blocking voltage of 790V, Appl. Phys. Express 8 (2015) 71001. http://dx.doi.org/10.7567/APEX.8.071001.

[9] T. Teraji, Y. Garino, Y. Koide, T. Ito, Low-leakage p-type diamond Schottky diodes prepared using vacuum ultraviolet light/ozone treatment, J. Appl. Phys. 105 (2009). http://dx.doi.org/10.1063/1.3153986.

[10] Y. Yamamoto, S. Harada, K. Seki, A. Horio, T. Mitsuhashi, D. Koike, M. Tagawa, T. Ujihara, Low-dislocation-density 4H-SiC crystal growth utilizing dislocation conversion during solution method, Appl. Phys. Express 7 (2014) 2–5. http://dx.doi.org/10.7567/APEX.7.065501.

[11] F.A. Ponce, B.S. Krusor, J.S. Major, W.E. Plano, D.F. Welch, Microstructure of GaN epitaxy on SiC using AlN buffer layers, Appl. Phys. Lett. 67 (1995) 410. http://dx.doi.org/10.1063/1.114645.

[12] C.R. Miskys, M.K. Kelly, O. Ambacher, G. Martínez-Criado, M. Stutzmann, GaN homoepitaxy by metalorganic chemical-vapor deposition on free-standing GaN substrates, Appl. Phys. Lett. 77 (2000) 1858. http://dx.doi.org/10.1063/1.1311596.

[13] T. Teraji, T. Yamamoto, K. Watanabe, Y. Koide, J. Isoya, S. Onoda, T. Ohshima, L.J. Rogers, F. Jelezko, P. Neumann, J. Wrachtrup, S. Koizumi, Homoepitaxial diamond film growth: high purity, High crystalline quality, isotopic enrichment, and single color center formation, Phys. Status Solidi 212 (2015) 2365–2384. http://dx.doi.org/10.1002/pssa.201532449.

[14] T. Hashizume, J. Kotani, H. Hasegawa, Leakage mechanism in GaN and AlGaN Schottky interfaces, Appl. Phys. Lett. 84 (2004) 4884–4886. http://dx.doi.org/10.1063/1.1762980.

[15] J. Rennie, M. Onomura, S. Nunoue, G. Hatakoshi, H. Sugawara, M. Ishikawa, Effect of metal type on the contacts to n-type and p-type GaN, J. Cryst. Growth 189–190 (1998) 711–715. http://dx.doi.org/10.1016/S0022-0248(98)00267-X.

[16] T. Sawada, Y. Ito, N. Kimura, K. Imai, K. Suzuki, S. Sakai, Influence of inhomogeneous barrier on I-V characteristics of metal/GaN Schottky diodes, Proc. Int. Work. Nitride Semicond. IPAP Conf. Ser. 1 (2000) 801–804.

[17] K. Shiojima, T. Sugahara, S. Sakai, Large Schottky barriers for Ni/p-GaN contacts, Appl. Phys. Lett. 74 (1999) 1936. http://dx.doi.org/10.1063/1.123733.

[18] T. Aoki, N. Kaneda, T. Mishima, K. Shiojima, Alternating current operation of low-Mg-doped p-GaN Schottky diodes, Thin Solid Films 557 (2014) 258–261. http://dx.doi.org/10.1016/j.tsf.2013.08.039.

[19] K. Shiojima, H. Wakayama, T. Aoki, N. Kaneda, K. Nomoto, T. Mishima, High-temperature isothermal capacitance transient spectroscopy study on SiN deposition damages for low-Mg-doped p-GaN Schottky diodes, Thin Solid Films. 557 (2014) 268–271. http://dx.doi.org/10.1016/j.tsf.2013.11.031.

[20] K. Shiojima, T. Sugahara, S. Sakai, Current transport mechanism of p-GaN Schottky contacts, Appl. Phys. Lett. 77 (2000) 4353. http://dx.doi.org/10.1063/1.1332981.

[21] S.M. Sze, Physics of Semiconductor Devices, 2nd ed, Wiley, New York, 1981, pp. 245–311.